μSR and its Application to Type-II Superconductivity

Tim Branch, Dong Chen, Graham Johnstone, and Konstantin Weisenberger
(Dated: November 22, 2019)

μSR is a spectroscopic technique which uses muon spin as a probe to measure the local magnetic properties of a sample [1]. Over the course of a muon's lifetime (2.2 μs) it will implant into a sample and its spin will precess about the direction of an applied and/or internal magnetic field. The positrons emitted in the decay are counted on a detector with the incident momentum direction characterizing the muon spin at the moment of production. Due to their small magnetic moment compared to that of an electron, muons are exceptionally useful in the study of magnetic samples because they will not influence ordered states. In combination with the locality of the measurement this allows one to detect multi-phase, short-ranged or anti-ferromagnetic order. By comparing characteristic properties of the spectrum to theoretical predictions even quantitative information about the magnetic properties can be extracted [2]. For these same reasons, the technique is well-suited for the study of superconductors [3]. In particular, the structure of the magnetic field distribution in the vortex state of a type II superconductor can be characterized, allowing properties such as the superconducting coherence length to be measured [3].

I. INTRODUCTION

μSR stands for "Muon Spin Relaxation/Resonance/Research", it is a collection of methods that use the muon spin to look at structural and dynamical processes in the bulk of a material on an atomic scale. It is functionally similar to resonance-based techniques like NMR and ESR. The essence of this bulk measurement is to utilize the muons magnetic moment along with its microsecond decay into a positron as a delicate tool to probe the local magnetic environment. Also, due to muon's small magnetic moment, they are an excellent probe for the study of exotic superconductors as they can penetrate into many types of materials without disturbing their properties as much as electron probes.

II. POLARIZED MUON PRODUCTION

There exist numerous high energy processes through which muons can be obtained. However, for the purposes of μSR, we are primarily interested in muons with low enough energy (4.119MeV) that they will become trapped in the sample over their short lifetime [1]. One available method to produce muons on this energy scale is through the following two-body pion decay process:

$$\mathrm{p} + \mathrm{p} \longrightarrow \pi^+ + \mathrm{p} + \mathrm{n}$$

With high-energy protons(>500MeV) hitting a production target, pions are produced. Pions with zero momentum in the lab frame undergo further decay into muons and neutrinos on the surface of the production target.

$$\pi^+ \longrightarrow \mu^+ + \nu_\mu$$

The weak interaction involved in this decay leads to a parity violation which forces the muon spin to always point in the direction opposite to its momentum. This property is the basis for μSR. The implication is that a muon beam is simultaneously guaranteed to be 100% spin-polarized - a significant improvement compared to other magnetic resonance probes. The necessity of this property will become clear in the following section.

At this point, it is worthwhile to mention that there exists an analogous decay process wherein π^- produces negatively charged muons, the probe for μ^-SR. However, this technique is rarely applied to systems in condensed matter [4]. Unless explicitly stated, 'muon' or 'μ' hereinafter will be used in reference to 'μ^+' for the sake of brevity. The principle difference between μ^- and μ^+ physics is where the muon implants in the sample.

A. Muon Implantation

The aforementioned μ^- carries a large mass in comparison to an electron. This leads it to preferentially cascade into the atomic 1s orbital so that it can minimize distance from the host nuclei. As this happens, there is a significant loss of spin polarization through radiation. This contributes unwanted signal noise. Depending on the Bohr radius of the μ^- orbit (recall that this is function of the atomic number Z), it is also possible to undergo the undesired fate of nuclear capture:

$$\mu^- + \mathrm{p} \longrightarrow \mathrm{n} + \nu_\mu$$

In direct contrast to the simplified understanding that μ^- has the physics of a 'heavy electron', μ^+ can be treated as a 'light proton'. As such, μ^+ generally implants at interstitial sites where the electron cloud is more dense. More specifically in regards to the high-T_C cuprates, there exist μ^+ stopping sites at a distance

$\sim 1\mathring{A}$ from oxygen ions [5]. One method of performing this calculation is to treat the μ^+-cation interactions with a screened coulombic potential and the μ^+-O^{2-} interaction as a Morse-like potential

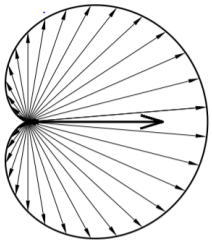

FIG. 1. The angular distribution of emitted positrons with respect to the initial muon-spin direction [1].

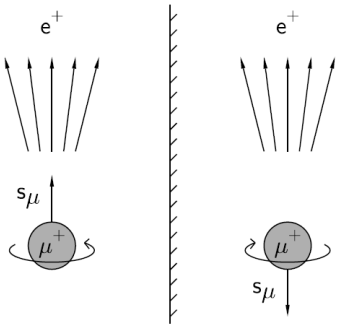

FIG. 2. Muon spin and the momentum of most energetic positrons [1].

$$V = 14.4\left(-\frac{a}{r} + \frac{b}{r^c}\right). \quad (1)$$

Where a,b,c are semi-empirical constants that are derived under the assumption that the net charge of the unit cell is zero. This is implies that we should only consider potential energy contributions from ions within the unit cell. Another general method for identifying muon sites is to employ a Monte-Carlo method that simulates the muon's thermalization process.

III. SPIN PRECESSION AND PARITY VIOLATION

Muons carrying a magnetic moment will precess in a magnetic field (either internal or external with respect to the sample) with frequency:

$$\omega = \frac{eg}{2m_\mu}B = \gamma_\mu B,$$

where γ_μ is the gyromagnetic ratio of the muon. Muons naturally decay into positrons after a lifetime of 2.2 μs, The angular distribution of emitted positrons is shown in Figure 1

$$\mu^+ \longrightarrow e^+ + \nu_e + \overline{\nu_\mu}$$

since this decay involves weak interactions, the parity symmetry is again violated, and that is why only the left in Figure 2 is observed in our universe.

IV. DETECTION

A. Detection mechanism

A schematic diagram for μSR is shown in Figure 3. Before a polarized muon (recall that muon spin is antiparallel with momentum) encounters the sample, it passes counter M. This activates an electronic "clock" with high time resolution (∼1 ns) that stops once a positron is detected. The positrons are emitted preferentially along the

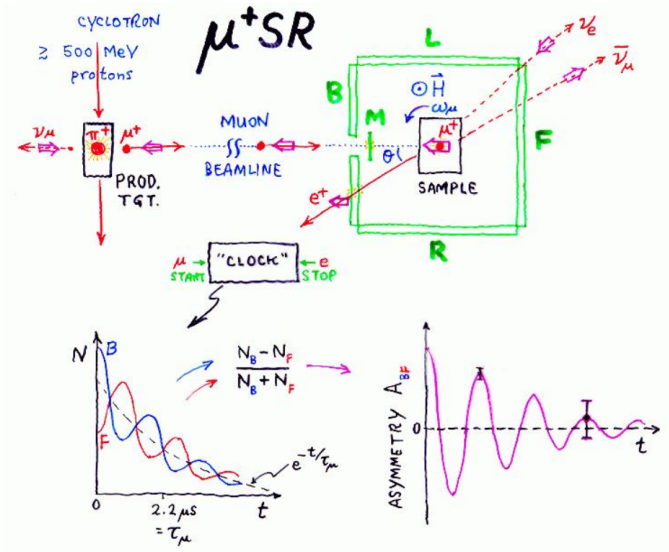

FIG. 3. Schematic experimental set up [6].

direction of muon spin at a given instant and are detected by one of the B-Backward, F-Forward, L-Left, R-Right detectors. The clock serves two purposes: (1) Account for random deviations from the average muon lifetime, and (2) subtract the signal contribution from any positrons produced by muons which decay before they reach the sample (i.e. 'in-flight'). Figure 4 shows that muons can be delivered to the sample and generate a time spectrum N(t) for each positron detector in one of two ways: as a continuous wave (CW) or a pulsed wave (PW). For CW, each muon will have its own clock. This provides good resolution in time at the cost of taking measurements slowly when compared to PW. In PW, many muons are released at a single instant in time such that there will be more detection events. However, each of these detections will carry poor time resolution. The spectrum collected by opposite detectors (B,F or L,R) are out of phase by 180 degrees and can therefore illustrate the precessing frequency of muons. Note that it is the momentum (trajectory) of the positron that is mapped to the muon spin. As long as the trajectory of positron is unaffected, its own

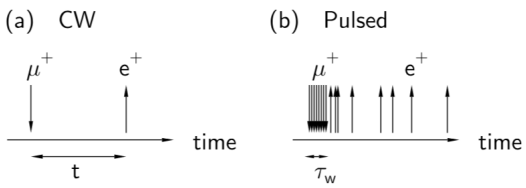

FIG. 4. Continuous wave vs pulsed wave.

spin precession in the magnetic field will not change N(t).

The following asymmetry function is presented to better illustrate the mapping of muon precession frequency to detection count N at F and B detectors:

$$A = \frac{N_B - N_F}{N_B + N_F} \tag{2}$$

It should be clear that as time evolves, the number of counts decreases exponentially, which result in a larger error bar for detections at larger t.

B. Detection Classification

While there are a multitude of μSR spectroscopy techniques, they can mainly be classified into 4 categories using 2 different parameters. The first is the previously mentioned muon beam configuration: CW vs. PW. The second is the direction of external magnetic field applied relative to the muon polarization: transverse field (TF) vs. longitudinal field (LF).

We will primarily focus on the design of Transverse Field Muon Spin Rotation (TF-μSR) and Longitudinal Field Muon Spin Relaxation (LF-μSR) using CW muon beams. These are commonly used in the study of type-II superconductors, and CW muon beams are used at TRIUMF.

1. Longitudinal Field Muon Spin Relaxation (LF-μSR)

To reiterate an important point from earlier, the implanted muons will precess in the applied field and produce a positron with momentum along the direction of the muon spin at a given moment. Counting these decay events over time generates a characteristic asymmetry pattern. This configuration can also be used to gather information about the weak internal magnetism in what is called zero-field muon spin relaxation (ZF-μSR). The capability of measuring local ordered magnetic moments without the need for an external field is an impressive feature of μSR which separates it from other magnetic resonance techniques.

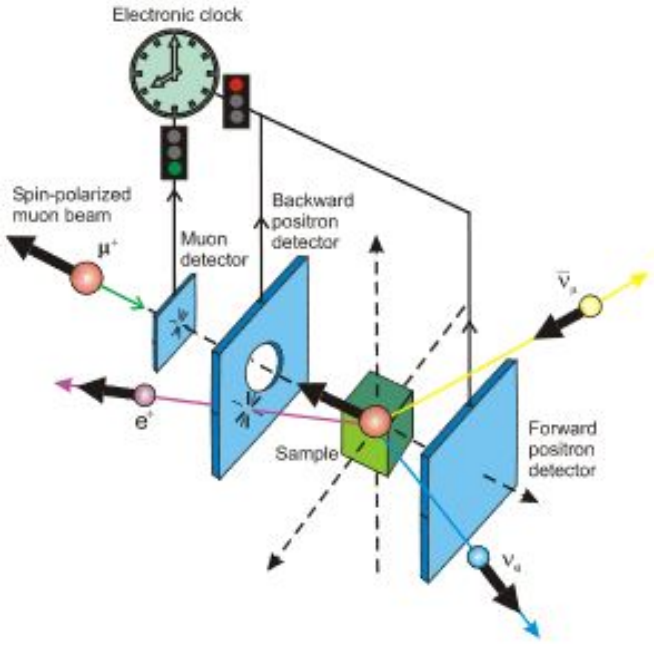

FIG. 5. Longitudinal Field (LF) μSR Setup [4].

2. Transverse Field Muon Spin Rotation (TF-μSR)

Similar to LF-μSR, the muons in a transverse field will precess with a frequency proportional to the strength of the applied field. This configuration is especially useful for studying type-II superconductors because it can measure the field distribution of the vortex lattice. For metallic systems, it can also be used to detect the 'Knight shift', which manifests as a fractional difference between the effective field produced at the muon site and the externally applied field.

V. APPLICATIONS

A. Magnetism

One well-established application of muon spectroscopy is the measurement of magnetic order in material. Muons are suited for studying magnetism since their magnetic moment γ_μ is large enough to measure small magnetic fields, but small enough not to influence the field of the sample. In experiments, muons are implanted uniformly across the unit cells of the sample where they couple to the local magnetic fields. The strength of the received signal from areas with the same magnetic order is then proportional to the volume occupied by the respective phase. I.e. the signal is not simply averaged over the whole sample, but there is a signal for each different type of magnetic domain. By analyzing the resulting asymmetry function it is possible to detect short-range or multi-phase magnetic order.

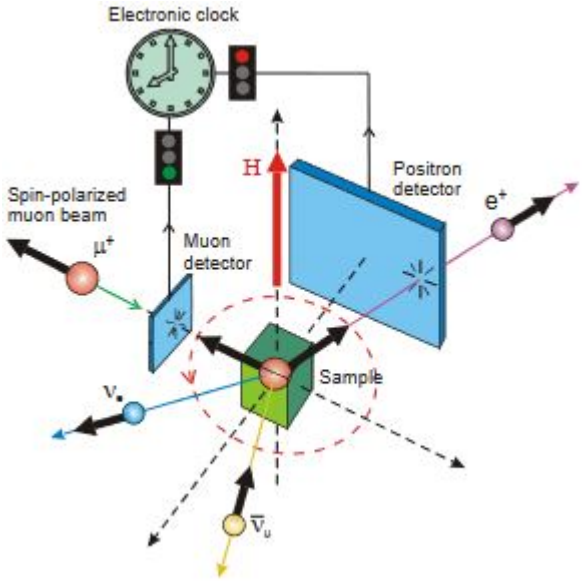

FIG. 6. Transverse Field (TF) μSR Setup [4].

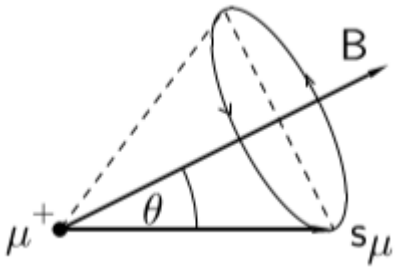

FIG. 7. The muon spin precesses in the applied magnetic field B. The inital spin at the time $t = 0$ and the field enclose the angle θ [1].

One disadvantage of this method, compared to techniques such as neutron diffraction, is that no spatial information is obtained. Also, data obtained from the muon relaxation function can not always be interpreted straightforward in a quantitative way. Since there are preferred muon sites in crystals, one must calculate the magnetic field at all possible muon sites and then choose the one consistent with observed data. In some cases, there are multiple preferred muon sites, as demonstrated in [7].

To understand the functional form of the spin asymmetry function we consider a muon with its spin $\vec{s}_\mu$ polarized in the z-direction in the local magnetic field $\vec{B}$ of the probe, as shown in Figure 7. The muon spin performs Larmor precession on a cone with the angle θ between $\vec{s}_\mu$ and $\vec{B}$. Since the asymmetry function (2) can also be interpreted as the projection of the spin on its initial polarization, we can construct it from the dynamics of the Larmor precession as

$$G(t) = \frac{B_z^2}{B^2} + \frac{B_x^2 + B_y^2}{B^2} \cos\left(\gamma_\mu |\vec{B}| t\right) \tag{3}$$

with the magnetic field $\vec{B} = (B_x, B_y, B_z)$ and the normalized asymmetry $G(t) = A(t)/A_0$. For all times with $\cos\left(\gamma_\mu |\vec{B}| t\right) = 1$ we recover $G(t) = 1$ and the spin polarization is back in its initial direction. Inserting the components of the magnetic field in spherical coordinates yields

$$G(t) = \cos^2\theta + \sin^2\theta \cos\left(\gamma_\mu |\vec{B}| t\right). \tag{4}$$

For a single crystal and a given muon site, the angle θ determines the whole observed spectrum of $G(t)$. In this case the asymmetry describes an oscillation around a baseline value.

One way of simplifying measurements is by using powdered samples. In such a probe, the angles between the muon spins and the magnetic field are distributed uniformly, meaning one can simply average over θ. The result is

$$G(t) = \frac{1}{3} + \frac{2}{3} \cos\left(\gamma_\mu |B| t\right). \tag{5}$$

In a sample, the local magnetic fields can fluctuate around their average since the electron spins couple to the randomly distributed nuclear spins. All of these fluctuations are uncorrelated, so using the central limit theorem one can argue that they follow a Gaussian distribution. We assume it is centered around zero with width Δ/γ_μ in all spatial directions. Averaging over all three components of the magnetic field results in

$$G(t) = \frac{1}{3} + \frac{2}{3} \exp\left(\frac{-\Delta^2 t^2}{2}\right)(1 - \Delta^2 t^2). \tag{6}$$

This result is known as the Kubo-Toyabe formula and was first derived 1967 [2]. As seen in Figure 8, it first decreases to an minimum and then relaxes to the"1/3-tail". Since this theory assumes static fields, having this tail in experimental data is an indicator for the absence of dynamics. This functional behaviour is often observed in materials, for example in the paramagnetic phase of the superconductor UCoGe at zero field by Visser *et al.* 2008 [8].

Measurements can be improved by applying a longitudinal field B_L in the direction of the initial muon polarization. For random internal fields, the longitudinal field shifts the mean of the Gaussian in z-direction from $\langle B_z \rangle = 0$ to $\langle B_z \rangle = B_L$. The asymmetry function takes the following form [9]:

$$G(t) = 1 - \frac{2\Delta^2}{B_L^2 \gamma_\mu^2}\left(1 - \cos\left(\gamma_\mu |B_L| t\right) e^{\left(\frac{-\Delta^2 t^2}{2}\right)}\right) \tag{7}$$

$$+ \frac{\Delta^4}{B_L^3 \gamma_\mu^3} \int_0^t \sin\left(\gamma_\mu |B_L| \tau\right) e^{\left(-\frac{-\Delta^2 \tau^2}{2}\right)} \mathrm{d}\tau. \tag{8}$$

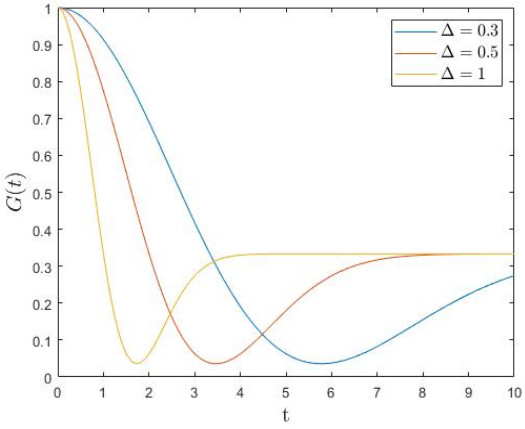

FIG. 8. The Kubo-Toyabe relaxation function for multiple values of Δ. For higher values of Δ, the relaxation to 1/3 takes longer.

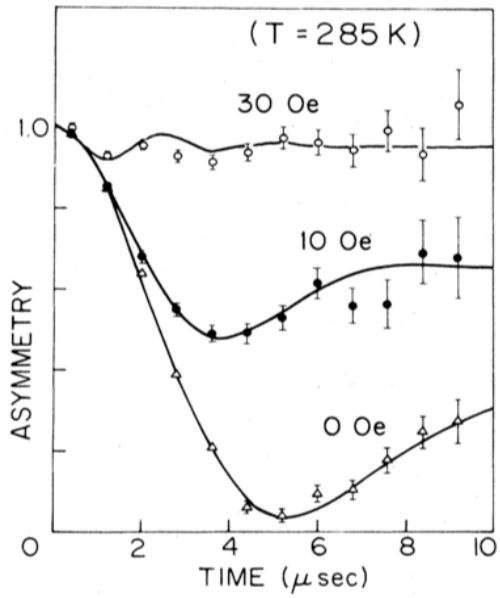

FIG. 9. The asymmetry function for MnSi in a longitudinal field. The fits match Eq. 8, suggesting the absence of dynamics.

With growing longitudinal field, the spin gets pinned stronger into the z-direction, causing the relaxation to be weaker. An example of this function was measured by Hayano *et. al* 1979 in MnSi at room temperature, as demonstrated in Figure 9.

The Kubo-Toyabe theory was derived for systems with static muons and electrons. This is the case for many, but not all materials of interest. One mechanism that can cause muon dynamics is so-called muon hopping, where they travel through different sites before they decay. If this is the case, the signal becomes an overlap of the signals from many possible muon sites. The result is an effective damping of $G(t)$. A similar effect could also be caused by impurities in the sample, making the interpretation of measurements difficult. Since each effect couples differently to the longitudinal field, measuring the oscillation frequency at high fields can distinguish the causes of de-phasing. This method helps to further characterize the material.

B. Probing of Magnetism in Superconductors

Superconductors are materials which have an identically zero resistivity below a critical temperature T_c, in sufficiently low magnetic fields[10]. Perhaps more importantly, they also expel magnetic fields from their bulk. The state in which these effects are seen is known as the Meissner state, and the magnetic field expulsion is known as the Meissner effect [10, Ch. 34]. Above the critical magnetic field $H_c(T)$ a conventional, or type I, superconductor will revert to the normal (non-superconducting) state, and the field will once again penetrate the sample [10].

Unconventional, or type II, superconductors exhibit an intermediate state known as the "mixed state". Below a lower critical field $H_{c1}(T)$ the sample completely expels all fields [10], and above the upper critical field $H_{c2}(T)$ it returns to the normal state, like a type I superconductor. When $H_{c1}(T) < H_{applied} < H_{c2}(T)$ thin filaments of flux are able to penetrate the sample as proposed by A. A. Abrikosov in 1957 [11]. This effect is shown in Figure 10.

It is important to note that in the Meissner state, as predicted by the London equations, magnetic fields are able to penetrate into the sample according to the form $B(x) = B_0 e^{-x/\lambda_L}$, where $\lambda_L = \sqrt{\frac{mc^2}{4\pi n_s e^2}}$ is the London penetration depth, and n_s represents the density of Cooper pairs within the superconductor [12][10]. As the distribution of muons implanted into the sample is know, the London penetration depth in this state can be measured using μSR [3].

Measurements of the penetration depth in the Meissner state allow the superfluid density n_s to be determined, which in turn provides valuable insight into properties such as the superconducting energy gap Δ. Ginzburg and Landau proceeded to build on the work of London and London by formulating a complex superconducting order parameter $\psi(\boldsymbol{r})$, the magnitude of which describes the degree of superconducting order at the position $\vec{r}$ [13][10].

The lattice of vortices within the mixed state results in an inhomogenous distribution of magnetic fields within the sample as shown in Figure 11 [3]. The variation of these fields is closely related to the change in the superconducting order parameter as a function of distance from the vortex core [10][3]. Using a variational model for the order parameter: $\psi(r) = r/\sqrt{r^2 + \xi_v^2}$ (where ξ_v is a variational parameter), the following analytic expression for the field distribution was produced, for the limit

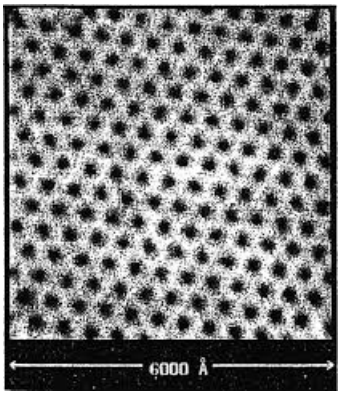

FIG. 10. Vortices in the mixed state of NbSe2 measured by scanning tunneling microscopy [14].

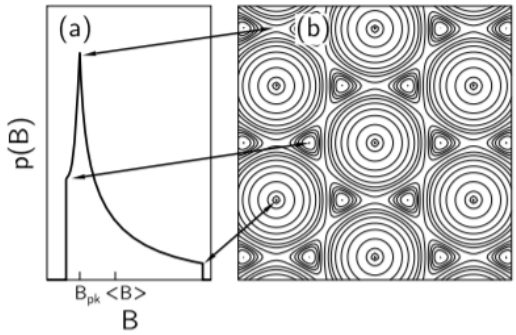

FIG. 11. Theoretically predicted magnetic field distribution for a hexagonal lattice of vortices. Inset: Contour plot of the magnetic field variation in space [3].

of isolated vortices (i.e. low fields) [3][15]:

$$\vec{B}(\vec{r}) = B_0 \sum_{\vec{K}} \frac{K_1(\xi_v\sqrt{K^2+\lambda_{ab}^{-2}})e^{-i\vec{K}\cdot\vec{r}}}{K_1(\xi_v/\lambda_{ab})\lambda_{ab}K}\hat{z}. \qquad (9)$$

In this equation, $K_1(x)$ is a modified Bessel function, λ_{ab} is the London penetration depth in the a-b plane, and $\vec{K}$ are the reciprocal-lattice vectors of the unit cell. It is assumed that the applied field is in the c-direction oriented along the $\hat{z}$-axis.

In the case of an extreme type-II superconductor, where $\lambda \gg \xi_{ab}$, it can be shown that $\xi_{ab} = \xi_v/\sqrt{(2)}$, where ξ_{ab} is the Ginzburg-Landau superconducting coherence length[3].

Muon spin measurements in YBCO demonstrate the changes in the magnetic fields as caused by these effects. Results are shown in Figure 12. Note that there is a small contribution from the maximum field strength, corresponding to the vortex cores; a moderate contribution from the minimum field points, corresponding to the points between three adjacent vertices; and a large contribution corresponding to the saddle points. To fit to physical parameters, a mathematical analysis similar to that performed in the works by Sonier and Clem are necessary

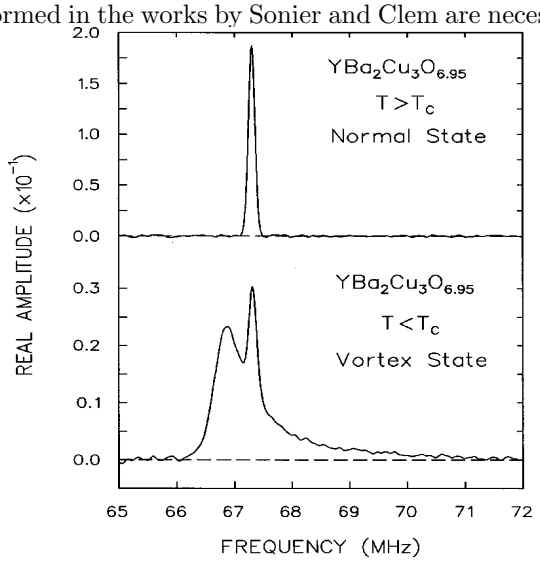

FIG. 12. Frequency plot of the muon spin precession signal of Yttrium Barium Copper Oxide (YBCO) measured in $\mu_0 H = 0.5$ T, in both the normal states (top panel, $T = 120$ K) and in the mixed state bottom panel, $T = 2.4$ K. [3]

to match such a distribution to the Fourier-transformed equation shown above, but will not be discussed here [15] [3].

VI. CONCLUSION

Due to the short effective range of its interactions with matter and the implantation mechanism of muons, μSR is a powerful technique. In less than a century since the discovery of the muon, several beam facilities have been built across the world [1]. this technique provides an alternative method for measuring the London penetration depth and superconducting coherence length thereby deepening our understanding on the high-Tc superconductivity. In the field of Magnetism, Kubo-Toyabe-Theory was developed based on the spectrum of asymmetric function of powder magnetic materials.

[1] S. J. Blundell, Contemporary Physics **40**, 175 (1999).

[2] R. Kubo and T. Toyabe, North-Holland, Amsterdam, 1967) p **810** (1967).

[3] J. E. Sonier, J. H. Brewer, and R. F. Kiefl, Rev. Mod. Phys. **72**, 769 (2000).
[4] J. Sonier, "μSR Brochure," (2002).
[5] W. K. Dawson, K. Tibbs, S. P. Weathersby, C. Boekema, and K. B. Chan, Journal of Applied Physics **64**, 5809 (1988).
[6] J. H. Brewer, "μsr: An introduction," (2009).
[7] J. Sugiyama, H. Itahara, J. H. Brewer, E. J. Ansaldo, T. Motohashi, M. Karppinen, and H. Yamauchi, Physical Review B **67** (2003), 10.1103/physrevb.67.214420.
[8] A. de Visser, N. T. Huy, A. Gasparini, D. E. de Nijs, D. Andreica, C. Baines, and A. Amato, Physical Review Letters **102** (2009), 10.1103/physrevlett.102.167003.
[9] R. S. Hayano, Y. J. Uemura, J. Imazato, N. Nishida, T. Yamazaki, and R. Kubo, Physical Review B **20**, 850 (1979).
[10] N. Ashcroft and N. Mermin, *Solid State Physics* (Saunders College, Philadelphia, 1976).
[11] A. Abrikosov, Journal of Physics and Chemistry of Solids **2**, 199 (1957).
[12] L. H. London F. and L. F. Alexander, Proc. R. Soc. Lond. A **149** (1935).
[13] V. L. Ginzburg and L. D. Landau, Zh. Eksp. Teor. Fiz. **20**, 1064 (1950).
[14] A. A. Abrikosov, Rev. Mod. Phys. **76**, 975 (2004).
[15] J. R. Clem, Journal of Low Temperature Physics **18**, 427 (1975).